NASA/TM-2019-104606/Vol. 54

Technical Report Series on Global Modeling and Data Assimilation, Volume 54

Randal D. Koster, Editor

Position Estimation of Atmospheric Motion Vectors for Observation System Simulation Experiments

David Carvalho, Will McCarty

August 2020

NASA STI Program ... in Profile

Since its founding, NASA has been dedicated to the advancement of aeronautics and space science. The NASA scientific and technical information (STI) program plays a key part in helping NASA maintain this important role.

The NASA STI program operates under the auspices of the Agency Chief Information Officer. It collects, organizes, provides for archiving, and disseminates NASA's STI. The NASA STI program provides access to the NTRS Registered and its public interface, the NASA Technical Reports Server, thus providing one of the largest collections of aeronautical and space science STI in the world. Results are published in both non-NASA channels and by NASA in the NASA STI Report Series, which includes the following report types:

- TECHNICAL PUBLICATION. Reports of completed research or a major significant phase of research that present the results of NASA Programs and include extensive data or theoretical analysis. Includes compilations of significant scientific and technical data and information deemed to be of continuing reference value. NASA counterpart of peer-reviewed formal professional papers but has less stringent limitations on manuscript length and extent of graphic presentations.

- TECHNICAL MEMORANDUM. Scientific and technical findings that are preliminary or of specialized interest, e.g., quick release reports, working papers, and bibliographies that contain minimal annotation. Does not contain extensive analysis.

- CONTRACTOR REPORT. Scientific and technical findings by NASA-sponsored contractors and grantees.

- CONFERENCE PUBLICATION. Collected papers from scientific and technical conferences, symposia, seminars, or other meetings sponsored or co-sponsored by NASA.

- SPECIAL PUBLICATION. Scientific, technical, or historical information from NASA programs, projects, and missions, often concerned with subjects having substantial public interest.

- TECHNICAL TRANSLATION. English-language translations of foreign scientific and technical material pertinent to NASA's mission.

Specialized services also include organizing and publishing research results, distributing specialized research announcements and feeds, providing information desk and personal search support, and enabling data exchange services.

For more information about the NASA STI program, see the following:

- Access the NASA STI program home page at http://www.sti.nasa.gov

- E-mail your question to help@sti.nasa.gov

- Phone the NASA STI Information Desk at 757-864-9658

- Write to:
  NASA STI Information Desk
  Mail Stop 148
  NASA Langley Research Center
  Hampton, VA 23681-2199

NASA/TM-2019-104606/Vol. 54

Technical Report Series on Global Modeling and Data Assimilation, Volume 54

Randal D. Koster, Editor

Position Estimation of Atmospheric Motion Vectors for Observation System Simulation Experiments

David Carvalho
CESAM-Physics Department, Aveiro University, Aveiro, Portugal

Will McCarty
Global Modeling and Assimilation Office (GMAO), NASA Goddard Space Flight Center, Greenbelt, MD

National Aeronautics and
Space Administration

Goddard Space Flight Center
Greenbelt, Maryland 20771

August 2020

Level of Review: This material has been technically reviewed by technical management.

Available from

NASA STI Program
Mail Stop 148
NASA's Langley Research
Center Hampton, VA
23681-2199

National Technical Information
Service 5285 Port Royal Road
Springfield, VA 22161
703-605-6000

Table of Contents

List of Figures

Abstract

An essential condition for a realistic Observing System Simulation Experiment (OSSE) is that the simulated observations provide a response similar to that of real observations within an atmospheric data assimilation system (ADAS). However, the simulation of some observations is complicated, going well beyond simply sampling a nature run at observation locations determined from real data. Atmospheric motion vectors (AMVs) are particularly complicated to simulate, given that their positions are determined from the location of tracers – cloud or water vapor features – that are, most likely, not instantaneously consistent between the underlying nature run and reality.

To address this issue, an algorithm for estimating the spatial distribution of atmospheric motion vectors (AMVs) was developed by the National Aeronautics and Space Administration (NASA) Global Modeling & Assimilation Office (GMAO). This algorithm is specifically for use in OSSEs with the final goal of estimating the impact of AMVs from new observing systems in the current Earth Observing System.

This report describes the algorithm used to determine the high-probability spatial locations where AMVs may exist based on where tracers exist within a nature run. First, the algorithm's ability to yield realistic observation counts and spatial distributions was assessed by using it to estimate AMV locations obtained by an existing instrument. This assessment showed that the AMV algorithm can successfully estimate realistic AMV locations for later use in OSSEs. Next, the AMV algorithm was used to synthesize AMV locations envisioned to be provided by MISTiC™ Winds, an Earth observing system concept. The report concludes by testing the MISTiC™ Winds Earth observing system concept as an example case.

1 - Introduction

Atmospheric motion vectors (AMVs) are estimates of wind speed and direction obtained from the tracking of atmospheric features such as clouds and local water vapor anomalies. Traditionally, AMVs are derived using geostationary (GEO) and low-Earth orbit (LEO) satellite imagery given temporal and spatial resolution considerations. Satellite imagery provides AMVs at high spatial and temporal coverage for practically all atmospheric levels below the tropopause. AMVs constitute a crucial source of tropospheric wind information for numerical weather prediction (NWP) models, particularly over oceans and high latitudes, where conventional wind measurements are scarce (Forsythe, 2007). These data have been shown to have a positive impact on the performance of NWP model forecasts (Forsythe, 2007; Goerss et al., 1998; Soden et al., 2001).

AMVs are computed from satellite imagery taken from the operational network of GEO and LEO polar-orbiting satellites. Due to the differences in spatial and temporal coverage of these two classes of satellites, there is currently a latitudinal gap in coverage between 55° to 70° N and 55° to 70° S latitudinal bands (Lazzara et al., 2013) between the GEO data (low latitudes, between 50ºN and 50ºS) and LEO data (high latitudes, poleward of 70ºN and 70ºS). One proposed solution to cover this latitudinal gap has been to deploy new satellite constellations, which would orbit in formation, providing measurements with sufficient local temporal information to derive winds over the entire globe (e.g., Lazzara et al., 2013).

OSSEs (Observing System Simulation Experiments; Errico et al., 2013; Hoffman and Atlas, 2016) are a useful part of the planning and development stages of any new instrument to be added to the existing observation network, as they can estimate the potential added value of new observations to the present Earth observing system by quantifying their expected impact within an atmospheric data assimilation system (ADAS). An OSSE simulates observations made by instruments on planned, proposed, or hypothetical observing platforms before the envisioned observing systems are built or deployed. An atmospheric OSSE is a numerical experiment conducted with an ADAS, consisting of a data assimilation algorithm and an atmospheric NWP model.

The simulated observations that constrain the ADAS within an OSSE are expected to represent those obtained from the real global observing system. These “observations” are simulated using a free-running atmosphere simulation called a Nature Run (NR, Errico et al., 2013). Unlike NWP forecasts of the real atmosphere, where the forecast and analysis errors cannot be easily and reliably quantified because the true state of the atmosphere is unknown, the underlying true atmospheric state within an OSSE framework is known perfectly, as it is the NR itself. Thus, all errors and metrics pertaining to the forecasts and analyses can be explicitly calculated and quantified. This renders an OSSE as a rigorous, cost-effective, and powerful tool to estimate potential improvements in weather forecasting skills when a new instrument or meteorological data source is sought to be added to the current Earth observing system (Errico et al., 2013). Furthermore, OSSEs can provide the basis for testing and evaluating alternate configurations and deployment strategies, for optimizing observing strategies, and for preparing the ADAS for the utilization of new types of data (McCarty et al., 2010; 2017 and 2018). For the specific case of expensive and technically challenging remote sensing systems, an OSSE can be a cost-effective tool in mission planning.

In a properly designed OSSE, the envisioned observations are realistically simulated in terms of their observation counts, spatio-temporal distributions, and errors. For the specific case of generating simulated AMV observations, an algorithm has been developed by the Global Modeling and Assimilation Office (GMAO) at NASA Goddard Space Flight Center to identify locations where there is a high probability of successful AMV retrieval based on the NR fields relevant to AMV tracers – e.g. cloud and water vapor fields. These probabilities can then be tested and used to obtain the locations from which the NR wind fields can be sampled to simulate AMV observations with realistic spatial and temporal distributions. This algorithm consists of a tunable and flexible code able to generate AMV distributions specific to different input sampling strategies – strategies that reflect, for example different satellite orbit configurations or instrument scan geometries.

An important aspect of this approach is that it was specifically designed to simulate realistic AMV distributions from a simulated atmosphere for use in OSSEs. This would be fundamentally difficult to do via traditional feature-tracking algorithms. The effective resolution of the NR is less than that of many current and proposed underlying observing systems. This algorithm aims to identify and select AMV locations based on the tracer fields from the NR. Note that while several approximations and assumptions are made to account for shortcomings in the underlying NR, more complicated aspects – e.g. systematic errors related to the AMV processing itself – are not accounted for in the observation simulation. Methods to statistically mimic realistic observation errors have been addressed in previous studies (e.g. Errico and Privé, 2014) and extend beyond the scope of this report.

In addition to describing the algorithm, this report presents an example application of this tool – the AMV algorithm was employed to simulate AMVs of the MISTiC™ Winds (Midwave Infrared Sounding of Temperature and Humidity in a Constellation for Winds) concept (Maschhoff et al. 2016). As an attempt to fill in the AMV latitudinal gap of the global wind observing system, multiple groups have proposed the concept of extending the AMV retrieval towards the mid-troposphere by the incorporation of moisture features tracking retrieved on pressure surfaces. To achieve this relative to existing imaging methods, a significant increase in spectral resolution both in temperature and moisture sounding channels is necessary; to achieve this relative to existing sounding methods, an increase in spatial resolution is necessary. However, an approach for producing AMVs on retrieval surfaces has been illustrated over the poles by Santek et al. (2014). MISTiC™ Winds is an observing system concept that consists of a constellation of small satellites equipped with miniature infrared (IR) spectrometers sampling near 4-6 μm to provide high spatial and temporal resolution temperature and humidity soundings of the troposphere. The envisioned observing strategy is to retrieve atmospheric state fields – temperature and moisture specifically – via a LEO constellation of satellites carrying the IR spectrometers. These temporally subsequent measurements can then be used to produce AMV retrievals on retrieved pressure surfaces of moisture.

Given that MISTiC™ Winds is still at a mission concept stage, OSSEs to evaluate the impact of MISTiC™ Winds observations on short- and medium-term weather forecast skill were performed at the GMAO (McCarty et al., 2017) based on the GMAO OSSE framework (Errico et al., 2013; Privé et al., 2013). All observations in this work were determined from the 7-km Goddard Earth Observing System version 5 (GEOS-5) Nature Run (G5NR, Gelaro et al. 2015). Note that pertinent aspects of the G5NR have been evaluated in previous work: Putman (2015) provides a general overview of the model, Privé et al. (2015) assess wind and temperature fields, Molod et al. (2015)

assess humidity and precipitation fields, and Norris et al. (2015) assess clouds and radiation. The present document describes the methods used to generate the AMV distributions of MISTiC^{TM} Winds from the G5NR for use in the OSSEs.

2 - Background and Motivation

The locations of AMVs fundamentally depend on the presence of trackable clouds and water vapor gradients (Velden and Bedka, 2009). Within a global OSSE, however, it is not feasible to detect and track clouds and water vapor features in the output of present-day NRs, either in model geophysical space or radiance space determined via radiative transfer calculations. Even with a 7-km global resolution, the G5NR grid is coarse compared to the spatial footprint of satellite imagery used in AMV retrieval, and the horizontal and vertical smoothing and dissipation in the G5NR results in an effective resolution several times coarser than the grid spacing. Thus, there are fundamental differences between real cloud and water vapor fields observed from space borne platforms and the simulated fields of any existing NR.

The main goal of an OSSE is to simulate observations that, when used in an ADAS, produces statistics and responses similar to those obtained with real observations. Therefore, a fundamental requirement of AMV simulation within an OSSE is to produce spatial and temporal distributions of wind retrievals that are representative of the real-world, assimilated datasets. However, the explicit extension of operational AMV retrieval methodology is not feasible. For the specific case of cloud-tracking AMVs, it is not feasible to perform target cloud identification and tracking using the cloud fraction fields of a NR, since cloud fraction fields do not represent actual clouds but rather contain only information about the fraction of a grid-cell covered by clouds. Thus, it is not possible to identify sharp features like cloud edges, which are vital for the target cloud identification and selection process. Furthermore, there is no way to identify any kind of reference point to allow the tracking of the feature in sequential model grids. A similar rationale applies to water vapor features. Therefore, methods to compensate for the impossibility of feature tracking in the NR were designed to obtain a realistic number and distribution of AMVs that are fundamentally related to the underlying meteorology of the NR.

Note that because only assimilated observations need to be considered in an OSSE, it is not necessary to mimic the end-to-end AMV retrieval methodology for OSSE applications – it is not necessary to perform full end-to-end AMV simulation from the NR via radiative transfer, radiance inversion, and feature tracking. (Feature tracking has already been deemed infeasible anyway.) In addition, within the context of data assimilation, AMVs are assimilated as point-measured winds; the upstream processing certainly affects the character of the observations, but the assimilation solution itself knows little about the upstream retrieval process. The critical issue is whether the simulated observations realistically incorporate the main characteristics of the real observations – for the focus of this work, the spatio-temporal distributions.

The methods in this report generate AMV locations and distributions that are a function of the underlying meteorology of the NR while attempting to handle the shortcoming of the NR's relatively coarse resolution. Additionally, they are reflective of the retrieval-based approaches and implemented in a concept similar to MISTiCTM Winds. Although much simpler approaches could be followed to simulate AMV distributions, including ones that would not take into account the presence of trackable atmospheric features in the NR, that would tamper with the response of an ADAS since where such features exist is often where more interesting, rapidly changing, and unpredictable weather occurs (Errico et al., 2007; McCarty et al., 2012; McNally et al., 2002). This is a fundamental motivation for this work, as many previous methodologies to simulate AMVs for OSSEs interpolated the NR wind fields to the locations where the real AMVs were

retrieved. Therefore, the clouds or water vapor features of the NR were not accounted for in the AMV simulation (e.g., Boukabara et al., 2016, 2018a, 2018b; Errico et al., 2013; Masutani et al., 2012). Thus, a significant fraction of the simulated AMVs may reasonably be expected to be placed at locations where no traceable features exist in the NR. This would lead to a fundamental mismatch between the character of the simulated AMVs and those that exist in reality. By considering observations that are not linked to the underlying meteorology of the NR, there may a fundamental dissonance between the simulated AMVs and the underlying level of predictability associated with the regimes in which AMVs are commonly retrieved in reality. This would likely be detrimental to the realism of the OSSE.

Finally, the algorithm presented in this work creates an AMV distribution based on the NR, but it does not simulate or add observational error in the observation simulation process. While it is of paramount importance to simulate these errors before the simulated observations can be fully utilized in an OSSE, the simulation of such errors is beyond the scope of this report. The GMAO has developed a reliable and accurate algorithm to statistically estimate observational errors for many types, including AMVs. These methods are thoroughly described in Errico et al. (2016).

3 - Description of the AMV estimation algorithm

The AMV distribution algorithm estimates observation locations by detecting features analogous to the real AMV tracers (clouds and water vapor features) in the G5NR cloud fractions and relative humidity fields. As the algorithm is meant to simulate AMV for satellite concepts, the G5NR fields are used to identify trackable features at the observation level - at each footprint observed by the satellite instrument. The AMV algorithm is divided into three code modules (Fig. 1): the main module along with the cloud and the water vapor features simulation modules.

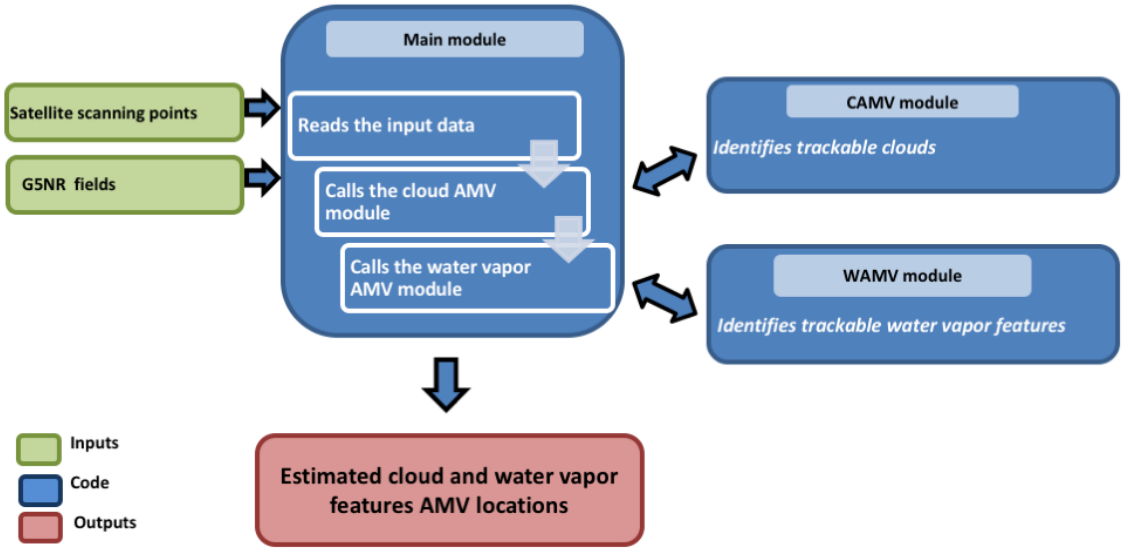

Figure 1 – Flow chart of GMAO AMVs algorithm code

The algorithm uses as input the satellite Level-1 observing spatiotemporal geolocation – specifically latitude, longitude, and time – and the G5NR atmospheric fields. AMV retrieval is fundamentally dependent on temporally sequential measurements to perform feature tracking. Since no feature tracking is actually performed in this algorithm, only the geolocation footprint for a single instrument flying in a single orbital plane is needed. For example, if a constellation of three satellites is sampling the same Earth-relative location to provide temporal sampling, only the center-flying satellite's ground sampling would be used.

Main module

The main module considers all radiance observation locations sequentially. At each scanning point, it collocates and subsamples the G5NR atmospheric fields for further processing. The main module determines the closest G5NR horizontal grid points to the instrument scanning spatiotemporal locations and samples the G5NR vertical columns at those points for the following variables: cloud fraction (CF), relative humidity (RH), pressure (p), tropopause pressure (ptrop), and the u and v components of the vector wind. These variables are then passed to the cloud AMV (CAMV) and water vapor AMV (WVAMV) modules.

CAMV module

The CAMV first determines how many independent clouds exist in each CF vertical column. Starting from the highest model level and moving towards the surface, a new cloud is considered when the CF exceeds 10%. Continuing to move downward, the lower bound of the cloud (the cloud base) is determined when the CF is again less than 10%. To each cloud or cloud layer, a pressure height following the European Organization for the Exploitation of Meteorological Satellites (EUMETSAT) methodology (Borde et al., 2014) is assigned. Specifically, for mid-to-high-level clouds with a cloud top pressure less than 700 hPa, the cloud pressure height is defined as that of the cloud top. For low level clouds with a cloud top pressure greater than 700 hPa, the cloud pressure height is defined as that of the cloud base.

The identified clouds are only considered at model levels, which are defined on a hybrid sigma-pressure coordinate (Gelaro et al., 2015). Since multiple layers of clouds may exist within a single G5NR vertical column, the cloud fraction of each cloud is determined using a maximum random overlap assumption (Tian and Curry, 1989). A trackable cloud is defined as one that: (i) is located below the tropopause, (ii) has a cloud fraction in the range of 20-80%, (iii) is not stationary (wind speed, U, greater than 3 ms-1), and (iv) is potentially viewable by the instrument. Regarding the final criterion, viewable means that the cloud is not substantially obscured by higher clouds. For this, the combined cloud fraction of all overlying cloud layers (CF_{above}), assuming a random overlap, must be less than 85%.

Once the trackable clouds are identified, a tunable probability function is used to determine which of those clouds will be selected as cloud AMV observation locations. Two issues motivate the use of this probability function. First, not all clouds present in the real atmosphere can be effectively tracked to derive AMVs, so by analogy, it is necessary to include in the AMV algorithm a method to select a subset of the identified trackable clouds. Second, the method employed here to identify trackable clouds does not account for the possibility of the horizontal extension of a given cloud across adjacent grid cells, or for the possible existence of independent horizontal clouds inside a given G5NR grid-cell, since only one cloud can be identified within a grid point vertical column at a given model level. Note that a given G5NR set of adjacent horizontal points at a given model level with positive cloud fractions can be considered as one of two distinct cases: either the model representation of a single cloud that extends horizontally; or the model representation of several independent clouds that are separated horizontally. Thus, the probability function is designed to address this uncertainty.

The cloud fraction-dependent probability function, $P_{(CF)}$, is shown in Figure 2. Clouds with CF in the ranges 0-20% are given a zero probability of AMV detection. The probability increases linearly from 0.2 to 0.4 for clouds with CF between 20% and 40%. For clouds with CF between 40 and 60%, a constant probability of AMV detection of 0.5 is assumed. For clouds with CF between 60% and 80%, the probability decreases from 0.4 to 0.2. Finally, for clouds with CF greater than 80%, a zero probability of AMV detection is assumed.

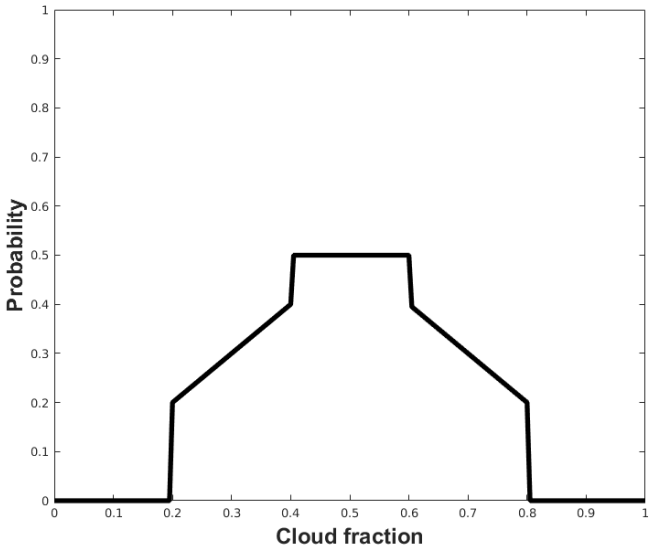

Figure 2 – Probability function P(CF)

For clouds with high CFs (> 80%), a zero probability is assigned because these clouds are likely to have few, if any, discernible edges, making it difficult to track the cloud due to the lack of reference points. This is illustrated in Figure 3, which shows real imagery of cloud-tracking AMVs obtained by the satellite Himawari-8. As can be seen in this real-atmosphere example, there are no AMVs in regions of opaque cloudiness. In fact, the cloud tracking AMVs are predominantly obtained in areas with smaller clouds and where cloud edges are distinct.

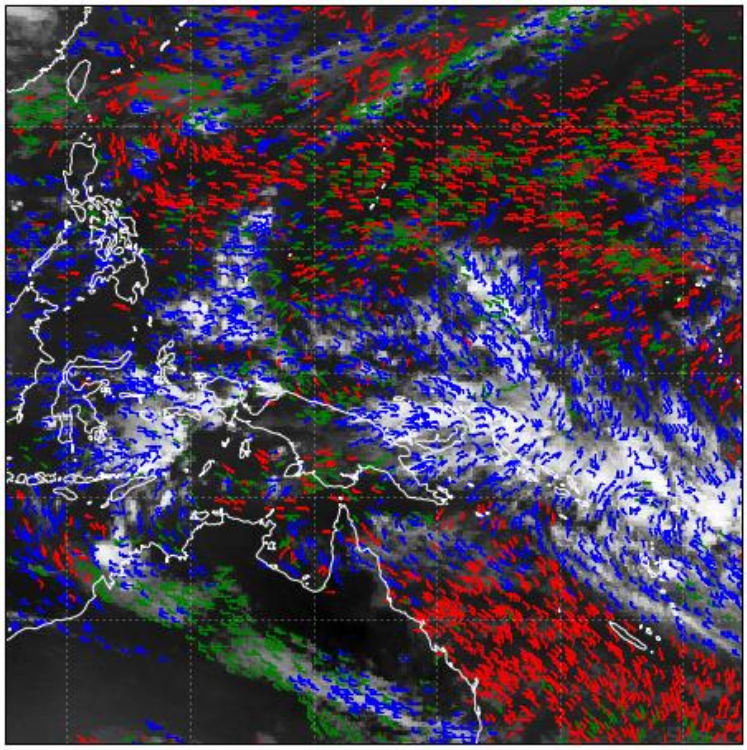

Figure 3 – Himawari-8 cloud-tracking AMVs. Red observations are located between 1000 and 700 hPa, green between 700 and 400 hPa and blue above 400 hPa

Finally, a tuning coefficient as a function of pressure height, b(p), was incorporated to inflate or deflate the probability function. Therefore, the final probability of a trackable cloud layer to be selected as an observation, P_c, is given by Eq. (1):

$$P_c(p, CF, p_{trop}, CF_{above}, U) = \begin{cases} 0 \;\; if p < p_{trop} \text{ or } |U| < 3ms^{-1} \text{ or } CF_{above} > 85\% \\ b(p) * P(CF) \;\; otherwise \end{cases} \quad (1)$$

For this case, a b(p) was defined for 6 vertical layers ranging in thickness from 100 to 150 hPa. The layers and b(p) are defined and adjusted to produce a realistic spatial and temporal distribution of AMVs. The final cloud AMV probability P_c is applied through the use of a random number R taken from a uniform distribution ranging from zero to one. For each trackable cloud layer, the trackable cloud feature is determined to be an observation location if $R < P_c$. Having determined the AMV observation locations as a function of latitude, longitude, height, and time, the corresponding observations can be determined from the G5NR wind fields.

WVAMV module

While the CAMV module allows the simulated AMV locations to be located at any of the G5NR native model vertical levels below the tropopause, the WVAMV module was designed to estimate AMV locations on retrieved isobaric moisture fields rather than in radiance space. The isobaric surfaces are specified as an input to the procedure and should be defined based on the spectral resolution and coverage of the instrument or instrument concept being studied. The natural coordinate of the G5NR is a hybrid-sigma coordinate. So, the relevant fields are interpolated by the WVAMV module to the prescribed isobaric levels while maintaining the native G5NR horizontal resolution.

Since water vapor feature tracking relies fundamentally on the presence of detectable, local relative humidity anomalies in the atmosphere, a scalar approximation of the RH gradient (RH_{grad}) is computed. This scalar gradient is defined as the difference between the maximum and minimum RH value within a 35 km x 35 km horizontal box and is used in place of the mathematical vector gradient. To illustrate the necessity for this gradient term, Fig. 4 shows real imagery of water vapor feature AMVs obtained by the satellite Himawari-8. As can be seen in this real-atmosphere example, WVAMVs tend to be located in regions with higher water vapor gradients. Note that this gradient estimation approach does not account for gradients for which the wind direction is perpendicular to the water vapor gradient, and this feature would thus appear stationary.

Each spatiotemporal observation location is tested at the closest G5NR horizontal grid point. A water vapor feature is considered trackable if it is not stationary (wind speeds > 3 ms^{-1}), is not substantially covered by clouds above (CF_{above} is less than 85%, assuming a vertical random overlap), and is located below the tropopause. Additionally, if cloud AMV observations were taken in that vertical column (i.e., if $P_c > R$ at that vertical column), no water vapor AMV observations will be taken below the highest cloud observation, since it is not likely that water vapor features will be observed below relatively opaque clouds.

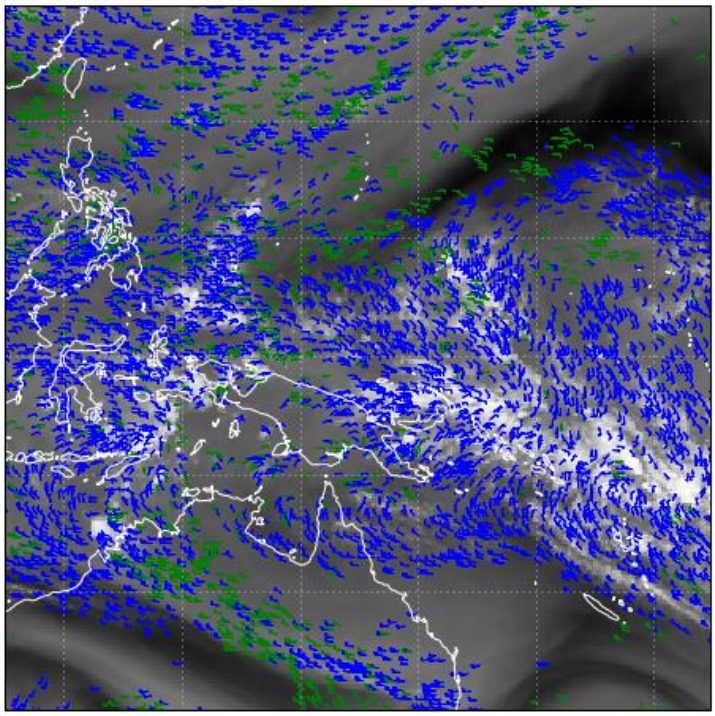

Figure 4 – Himawari-8 water vapor features tracking AMVs. Green observations are located between 700 and 400 hPa and blue above 400 hPa

In analogy to what was done for the CAMV, a tunable probability function, $P(_{RHgrad},CF)$, was included in the code to obtain a realistic spatial and temporal distribution of simulated WVAMVs. As part of this function, each point is considered to have a potentially trackable feature only if the RHgrad is higher than 65%. This function (Figure 5) gives higher probabilities to trackable water vapor features with higher RH_{grad} and to those less likely to be obscured by clouds above. An additional pressure-height tuning coefficient, c(p), is incorporated. The final probability of a trackable water vapor feature to be selected as a WVAMV location, P_{WV}, is:

$$P_{wv}(p, RH_{grad}, CF, p_{trop}, CF_{above}, U, P_C) = \begin{cases} 0 \; if \; p < p_{trop} \text{ or } |U| < 3ms^{-1} \text{ or } CF_{above} > 85\% \vee P_C > R \\ c(p) * P(RH_{grad}, \text{CF}) \; otherwise \end{cases} \quad (2)$$

For each pressure layer a c(p) value was defined and manually adjusted to produce a realistic spatial and temporal distribution of AMVs, both vertically and horizontally. A trackable water vapor feature is deemed as an observation if $R<P_{WV}$. Having determined the AMV observation locations, the G5NR wind fields can be sampled to obtain the water vapor-derived AMV observations for the OSSE.

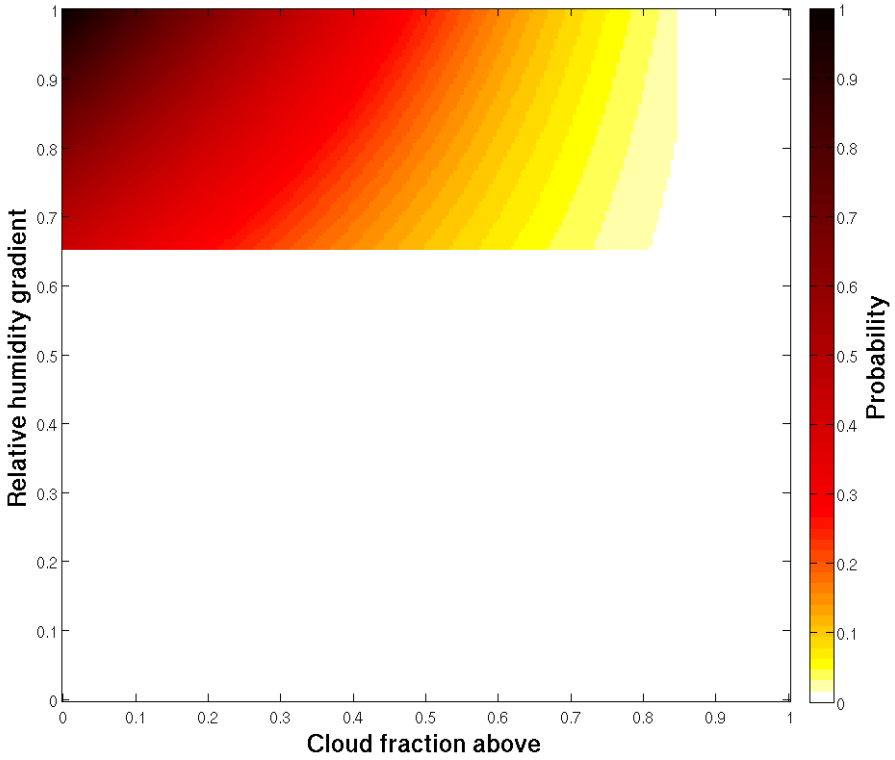

Figure 5 – Probability function P_{wv} as specified by RH_{grad} and CF_{above} values

One of the main reasons to include the tuning coefficients b(p) and c(p) in the CAMV and WVAMV probability functions, respectively, is to account for differences between the G5NR and the real atmosphere meteorology, which are expected to be a major source of discrepancies between estimated and real AMV distributions and locations. Gelaro et al. (2015) made an extensive validation of the G5NR cloud and humidity fields against a wide range of observations and reanalyses. They showed that the G5NR cloud spatial distributions do differ from those of the real atmosphere – although the G5NR cloud spatial distributions are realistic in a climatological sense, there are areas where the G5NR shows an excess (or lack) of clouds when compared to observations. Similar findings were reported for the humidity fields; in some regions, the G5NR appears to be too dry or too wet when compared to observations, though the overall humidity fields are considered realistic. By including the tuning coefficients in the probability functions, it is possible to tune the AMV estimated from the G5NR location counts and spatial distributions to match the real ones and thereby attenuate the explicit shortcomings in the G5NR cloud and humidity fields that can affect the realism of the identification and selection of AMV tracers from the G5NR.

4 - Assessment of NR-derived AMV distributions

The performance of the algorithm was assessed by comparing its AMV location estimations to those of a real instrument in the global observing system. Qualitatively, the cloud AMV locations need to be located at times and places in the G5NR where fractional cloudiness exists. The water vapor AMV locations need to be consistent with RH gradients.

For this, the Advanced Imager (AHI) on the Himawari-8 geostationary satellite was chosen. AHI is among the most advanced infrared imagers available in the global Earth observing system. AHI measures 16 spectral bands, with three bands measuring the 6.7 μm water vapor continuum and three bands measuring the 11 μm atmospheric window. The nominal resolution of these infrared bands is 2 km at nadir. The spatial resolution is at or exceeds that for envisioned future applications of this algorithm, though the spectral sampling is far inferior to those instrument concepts which propose sampling the water vapor AMVs on retrieved isobaric surfaces.

The AHI scanning points for the complete month of July 2015 were used as input to the AMV algorithm for the estimation of the AHI AMV locations. The cloud and water vapor modules' probabilistic functions b(p) and c(p) were tuned so that the estimated AHI AMV locations show a spatio-temporal distribution which was realistic compared to one of the real AHI AMV distributions.

Although Himawari-8 completes a full disk scan once every 10 minutes, the AHI AMV data streams assimilated in the GMAO forward processing system contain only three full disks of data within each six-hour assimilation window, corresponding to times of -1.5h, -0.5h and +0.5 hours relative to the center of the assimilation window. For example, AMV observations are available at 2230, 2330, and 0030 UTC for the six-hour assimilation window centered on 00:00 UTC. Himawari-8 scanning points where the viewing angle relative to the nadir location is larger than 60°, with longitudes eastward of 89° E and westward of 170° W, were discarded since no real Himawari-8 AMVs are operationally assimilated at these locations in the GMAO forward processing system.

Although July 2015 AHI scanning points are fed into the algorithm, AMV locations are estimated using the July 2006 G5NR atmospheric fields. This distinction in year does not affect the evaluation of the algorithm. There is no direct correspondence of July 2006 G5NR meteorology to the real-world meteorology of that time (aside from small effects associated with the prescription in G5NR of 2006 SSTs), as G5NR is a free-running atmospheric simulation. Gelaro et al. (2015) illustrated that the G5NR consists of weather events with realistic variability and climatology representative of the real atmosphere. In this sense, July 2006 in the G5NR can be regarded as a typical July. It is not expected that the simulated AHI AMV locations will directly match the real AHI AMV locations; rather, the goal is for the simulated AMV locations to show counts and spatiotemporal distributions that are similar to those of the real AMVs.

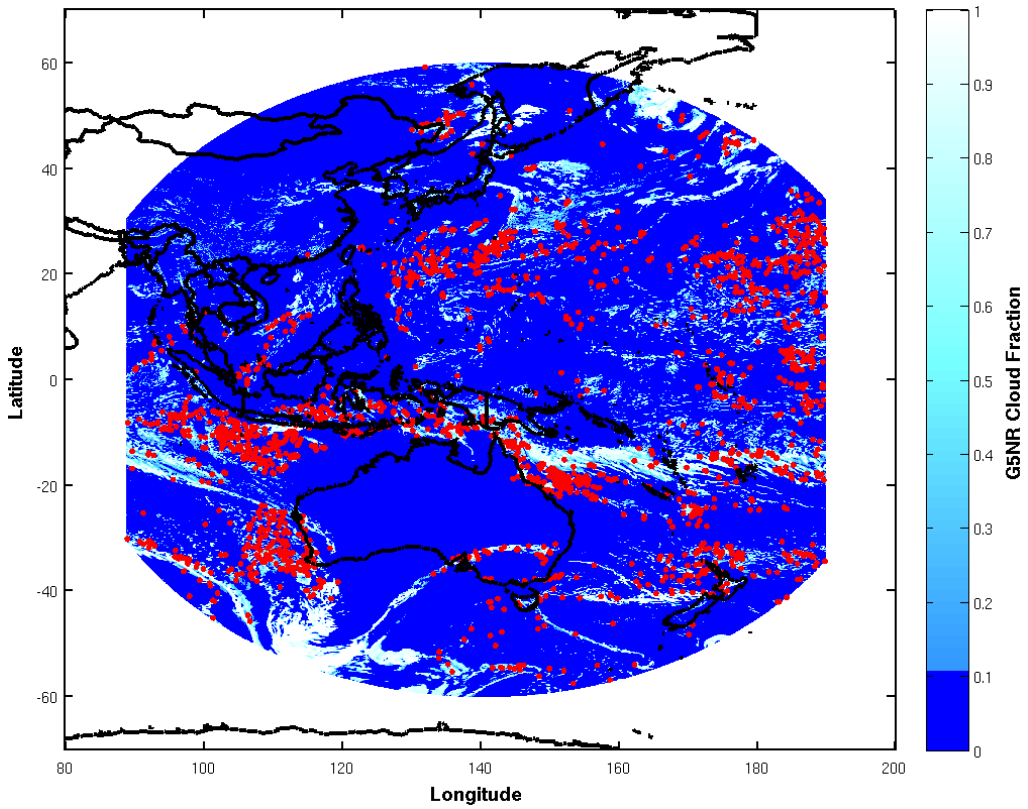

Figure 6 – Estimated Himawari-8 cloud AMV locations overlapped with the G5NR CF field at 900 hPa - 1 July 0030 UTC. Dark blue color (CF < 0.1) means that the sky is considered as cloud-free.

Figure 6 depicts the G5NR CF field at 900 hPa and G5NR-derived cloud AMV locations in a 50 hPa bin centered at 900hPa for 0030 UTC on 1 July 2006. The cloud AMV locations are seen to be physically consistent with the simulated clouds; they are mainly located where the G5NR points are fractionally cloud covered, i.e., where cloud edges should be more discernible.

The CAMV probability function P_c, described in section 3.2, gives higher probabilities to clouds with intermediate cloud fractions (40% to 60%). As seen in Figure 6, many areas with intermediate cloud fractions do not contain observation locations, while other areas with smaller or larger cloud fractions contain a considerable number of them. This happens for three reasons. The first is related to the very nature of the probability function – although it gives higher probabilities to clouds with intermediate cloud fractions and lower probabilities to clouds with small or large cloud fractions, there will still be AMV locations at places with small or large cloud fractions, albeit fewer in number. The second reason is that this vertical level may not correspond to the cloud pressure height determined for a cloud that extends over multiple model levels. As mentioned in section 3.2, the height for these low clouds is defined as the cloud base (based on Borde et al., 2014). In some clouds, the cloud base may extend below 900 hPa. Finally, even if a cloud has an intermediate cloud fraction, it might be obscured by other clouds above and thus be excluded by P_c as a possible AMV location.

Figure 7 shows the estimated AHI water vapor AMV locations within a 50 hPa bin centered at 200hPa (175-225 hPa) and the corresponding G5NR RH_{grad} field for 1 July 2006 00:30 UTC at 200 hPa. The shading of the RH_{grad} is discontinuous at 0.65 to illustrate the lower limit threshold of AMV detection described in section 3.3.

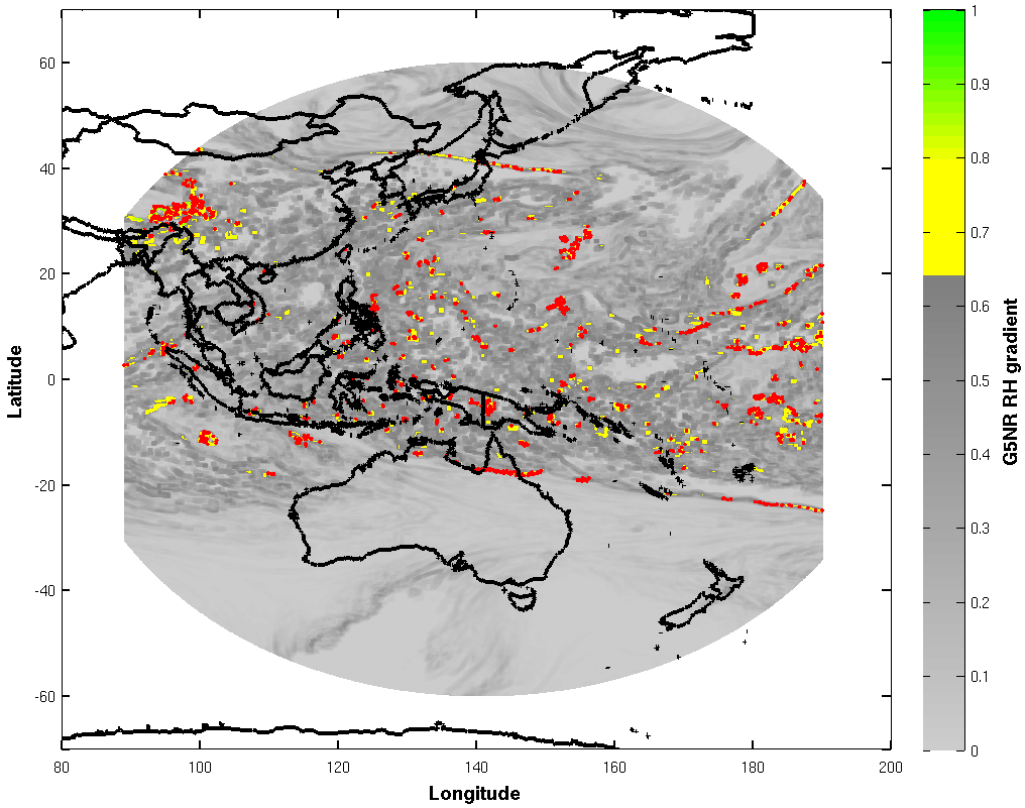

Figure 7 – Estimated Himawari-8 water vapor AMV locations overlapped with the G5NR RH_{grad} field at 200 hPa - 1 July 0030 UTC. RH_{grad} < 65% are colored grey since this was defined as the lower threshold for water vapor AMV detection.

By construction, the AMV algorithm derives water vapor AMV locations with physical realism, since they are estimated to be located at G5NR points where the RH_{grad} is above 65% (Fig. 7). Areas with high RH_{grad} that do not contain any observations occur due to the sampling of the probabilistic model or to the presence of opaque cloud decks above the moist regions (Section 3.3).

The estimated AMV monthly spatial distribution for Himawari-8 AHI is now compared to the real distribution obtained from the Modern-Era Retrospective analysis for Research and Applications, Version 2 (MERRA-2, Gelaro et al., 2016). Specifically, the distribution of the AMV estimated positions for G5NR July 2006 is compared to that for the actual July 2015 AHI AMV positions. Temporally, the G5NR AMV locations were estimated in a manner consistent with those assimilated in MERRA-2. Specifically, they were sampled every 2 hours over the six-hour analysis windows centered upon 0000, 0600, 1200, and 1800 UTC. For the results in this section, the P_c and P_{wv} probabilistic functions b(p) and c(p) were manually tuned so that the simulated AMV location distributions closely matched the real AHI AMV vertical distributions. For this comparison, the MERRA-2 real and G5NR estimated positions are aggregated spatially and vertically and considered in terms of counts per 6-hour analysis time, as shown in Figure 8. The spatial distributions represent an aggregation into 5° x 5° bins across all vertical levels, and the vertical distributions represent all spatial locations aggregated into 100 hPa bins.

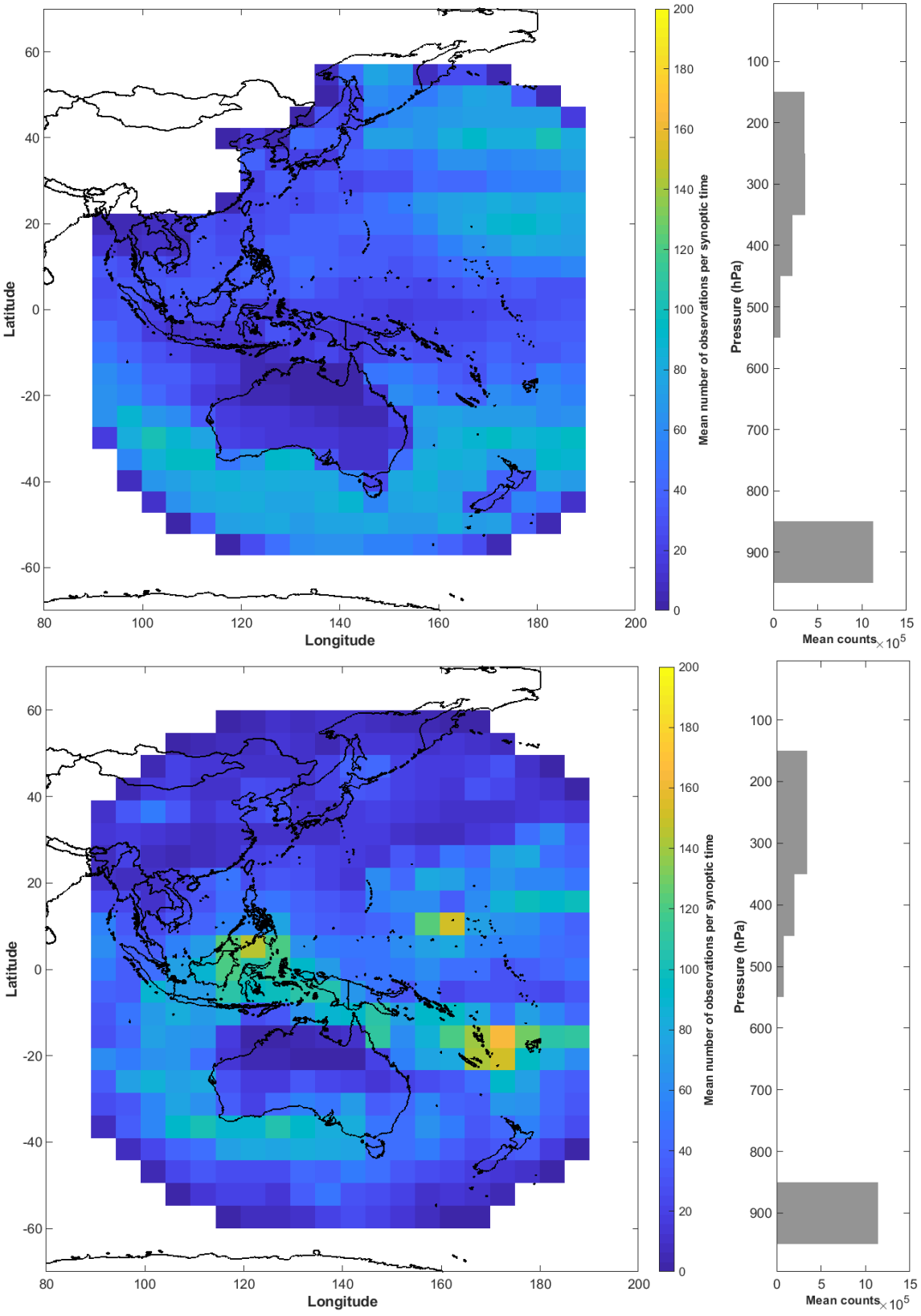

Figure 8 – Real (top) and simulated (bottom) AHI cloud AMVs. Spatial (left) and vertical distribution (right) for July 2015 (top) and July 2006 (bottom)

Figure 8 shows that the spatial and vertical distributions of the estimated AHI cloud AMV locations closely match the corresponding real distributions. The estimated observation counts per six hours (17,393) are in close agreement with the number from Himawari (17,253 AMVs). There

is strong agreement in the vertical distribution of the observation locations, with a bimodal structure showing maxima corresponding to high (400-200 hPa) and low (800-1000 hPa) clouds. The minimum in the mid-tropospheric AMV counts is related to the climatological distribution of cloud top height in pressure-space (Wylie and Menzel, 1999, McCarty et al., 2012), which generally restricts the majority of the cloud-derived AMVs to the upper- and lower-troposphere, with a gap in the mid-troposphere. Similarly, the spatial and temporal constraints have largely limited these methods to satellite imagery. Imagers measure improved spatial resolution at the expense of spectral resolution. Spectral resolution is akin to vertical resolution in radiance space. For water vapor features, this results in relatively few pieces of information (~2-3 spectral bands on the geostationary imagers, none on the operational polar orbiting imagers). By these constraints, the cloud- and water vapor-derived AMVs complement each other spatially, but their vertical distributions are largely non-complementary, resulting in a data void in the mid-troposphere.

The horizontal distributions show that the real cloud tracking AMVs tend to be scarcer over land and even non-existent over some inland areas of the Australian continent. This is not due to an instrument limitation or characteristic, but rather to the blacklisting of data over land areas. VIS and IR cloud-tracking AMVs below 400-500 hPa over land areas are usually blacklisted or given a low quality index (Lean et al., 2016) since these winds are influenced by topography and do not correspond with the general atmospheric flow (Cordoba et al., 2016). Often these lower level clouds have a short lifetime and size (Szantai et al., 2000). This quality control decision was not built into the CAMV module.

Over the ocean, the real cloud-tracking AMVs show higher counts compared to the estimated distribution between 30°S and 50°S and in the northeastern sector of the scanning disk. On the other hand, the estimated AHI AMV locations are higher in number than the real ones between, for example, Indonesia and Papua New Guinea. These differences in the horizontal distributions of the cloud AMVs stem from differences between the G5NR July 2006 meteorology and the real July 2015 meteorology and from the fact that the G5NR, as a simulation, has its own inherent limitations and deviations from reality. A detailed discussion and analysis of the differences between the real atmosphere and the G5NR cloud climatology is available in Gelaro et al. (2015), where an extensive validation and discussion of the G5NR cloud fields were made against the Clouds and the Earth's Radiant Energy System Single Scanner Footprints (CERES SSF) and the Cloud-Aerosol Lidar with Orthogonal Polarization (CALIOP) observations. These comparisons showed that the G5NR has excessive clouds over the Indonesian archipelagos including Papua New Guinea and adjacent areas, consistent with the results shown in Figure 8.

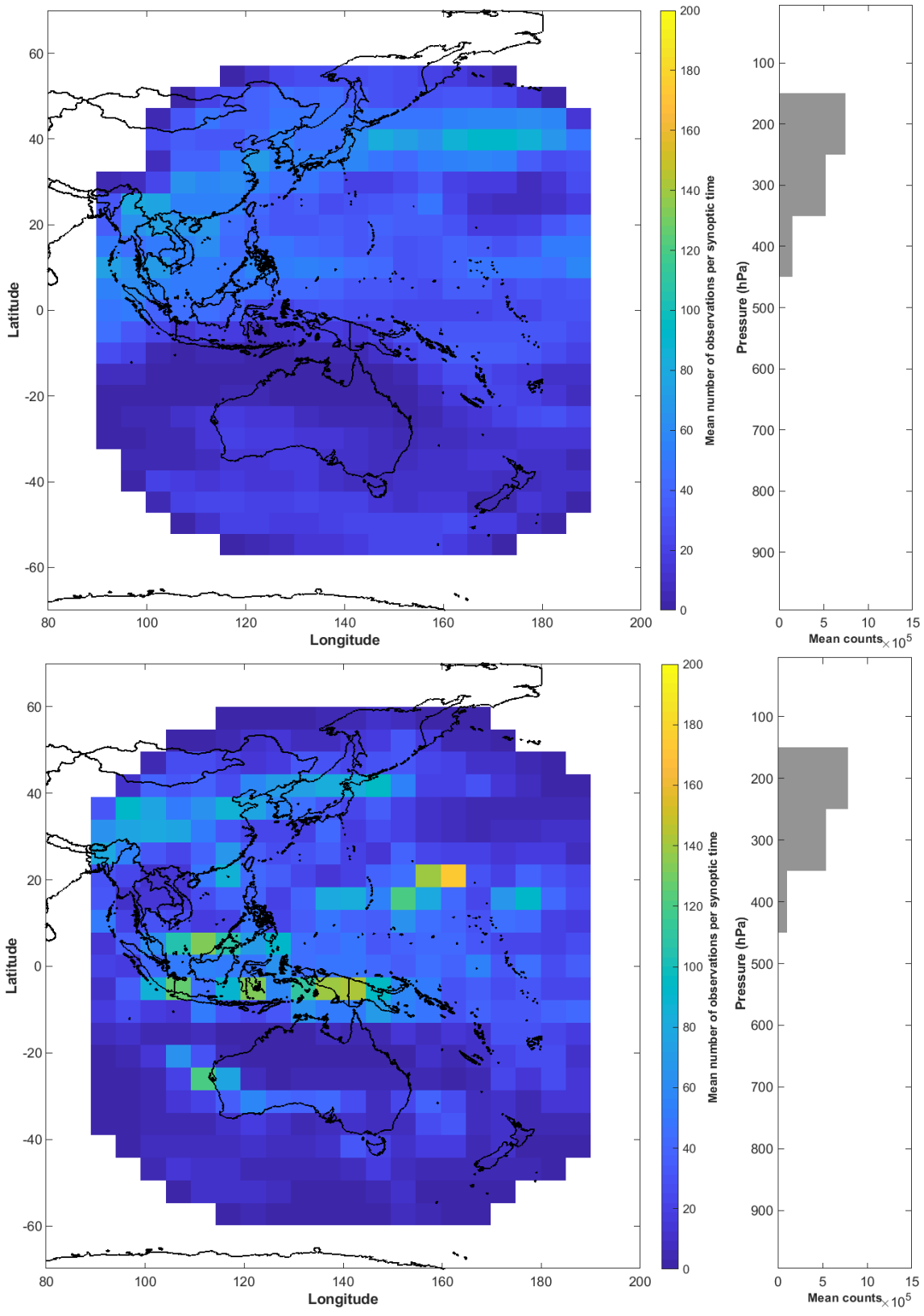

Figure 9 – Real (top) and simulated (bottom) AHI water vapor AMVs spatial (left) and vertical distribution (right) for July 2015 (top) and July 2006 (bottom).

Figure 9 shows the same information as Figure 8, but for the WVAMVs. As for the CAMVs, the simulated WVAMVs provide a good representation of the horizontal observation counts (11,560

estimated observations compared to 11,511 real observations for each 6-hour period), with very similar vertical distributions. Again, the simulated AMVs' minima and maxima locations do not match exactly. While both the simulated and real water vapor AMVs show minima for counts in the lower half of the Himawari-8 scanning disk, the estimated AMVs show maxima around the Indonesian archipelagos whereas the real AMVs' maxima are more widespread along the upper section of the satellite scanning disk. A validation of the G5NR humidity fields (Gelaro et al., 2015) showed that the G5NR has much higher total precipitable water (TPW) than the reanalyses (ERA-Interim and MERRA) in the June-July-August period over the areas surrounding the Indonesian archipelagos, which would explain the larger observation density in the simulated WVAMV observations there (Fig. 9).

Overall, despite some differences, the estimated cloud and water vapor AMV locations show a high degree of realism in terms of their spatial and temporal distributions. It can be concluded that the simulation algorithms estimate AMV locations with sufficient quality to provide a realistic simulated AMV dataset for assimilation, which is the main goal of an OSSE.

5 - Application of the AMV estimation algorithm to MISTiC™ Winds

To illustrate the utility of the algorithm, it is now used to identify and locate AMV tracers from the G5NR according to the envisioned performance of the MISTiC™ Winds constellation concept, based on the specs provided by BAE Systems (Maschhoff et al. 2016). Given that the AMV algorithm probability functions, Pc and Pwv, need to be tuned to obtain realistic counts and spatial distributions, a proxy instrument has to be used for the tuning. Since there are no observing systems in the current Earth observing system implementing the sounder derived, retrieval-centered AMV tracking strategy globally, the simulated MISTiC™ AMVs cannot be calibrated nor validated with a real counterpart in terms of counts and spatial distributions. AHI, however, though geostationary, has a similar horizontal resolution to MISTiC™ Winds. It is thus considered a suitable proxy instrument for the tuning, particularly for the cloud-derived AMV probability function.

Note that for WVAMVs, there is a fundamental disconnect between the simulation of the AHI AMV observation locations in the preceding section and the purpose of this algorithm. AHI water vapor AMVs are derived in radiance space and are assigned pressure-heights in order to translate them from radiance to physical space. The MISTiC™ Winds concept proposes to perform feature tracking on retrieved pressure surfaces, as made possible by its increased spectral coverage and resolution. Thus, a MISTiC™ Winds instrument can resolve water vapor gradients at varying levels due to its increased vertical information content. This strategy was an implicit target in the design of the AMV position estimation algorithm. In Section 4, no water vapor AMV locations were allowed to be estimated below 400 hPa similarly to AHI. For MISTiC™ Winds, water vapor AMV positions in the middle and lower-troposphere are considered and desired.

Other instruments that have equivalent input data to MISTiC™ Winds could be used as a proxy instrument, in particular the Atmospheric Infrared Sounder (AIRS) temperature and humidity profiles obtained by the Cooperative Institute for Meteorological Satellite Studies from the University of Wisconsin-Madison, as described in Santek et al. (2014). However, AIRS AMVs are currently still an experimental product. In addition, for OSSE applications, a proxy instrument should ideally already be part of an operational/forward processing system, with a good degree of knowledge already amassed about associated observational errors and data processing requirements. Also, the temporal spacing between subsequent scenes would be much larger with the AIRS AMV method; for AIRS, the spacing is akin to the period of the orbit (100 minutes), whereas that for the constellation strategy proposed in MISTiC™ Winds is on the order of standard geostationary processing scene separation, or ~15 minutes. Additionally, as previously mentioned, the spatial resolution of MISTiC™ Winds is akin to AHI, whereas the AIRS footprint spacing is in-line with traditional sounder spatial resolutions, 13.5 km. Finally, AIRS AMVs are retrieved only at polar regions whereas the MISTiC™ Winds coverage is global, which may result in differences when compared with tracers located at other latitudes, namely in terms of the cloud and water vapor features inherent characteristics and respective spatial distributions. For these reasons, AIRS was not chosen as the proxy instrument for calibration of the AMV algorithm when applied to MISTiC™ Winds.

Based on the MISTiC™ Winds spectral resolution and coverage, the fixed isobaric levels were defined in the WVAMV module at 150, 200, 250, 300, 400, 500, 600, and 700 hPa. A single orbital plane would provide spatial coverage comparable to current LEO satellites. However, the

constellation strategy would result in a temporal revisit that is otherwise not achieved through existing polar-orbiting platforms, at least not to the extent to fully utilize the observations for AMV retrieval over the entire orbit. Extending MISTiC™ Winds to four orbital planes would correspond to an improved global coverage of the constellation, though these simulated orbits may be somewhat suboptimal. It may be possible to further limit the observing gaps by adjusting the orbital parameters of each plane to limit the overlap across the different orbital planes.

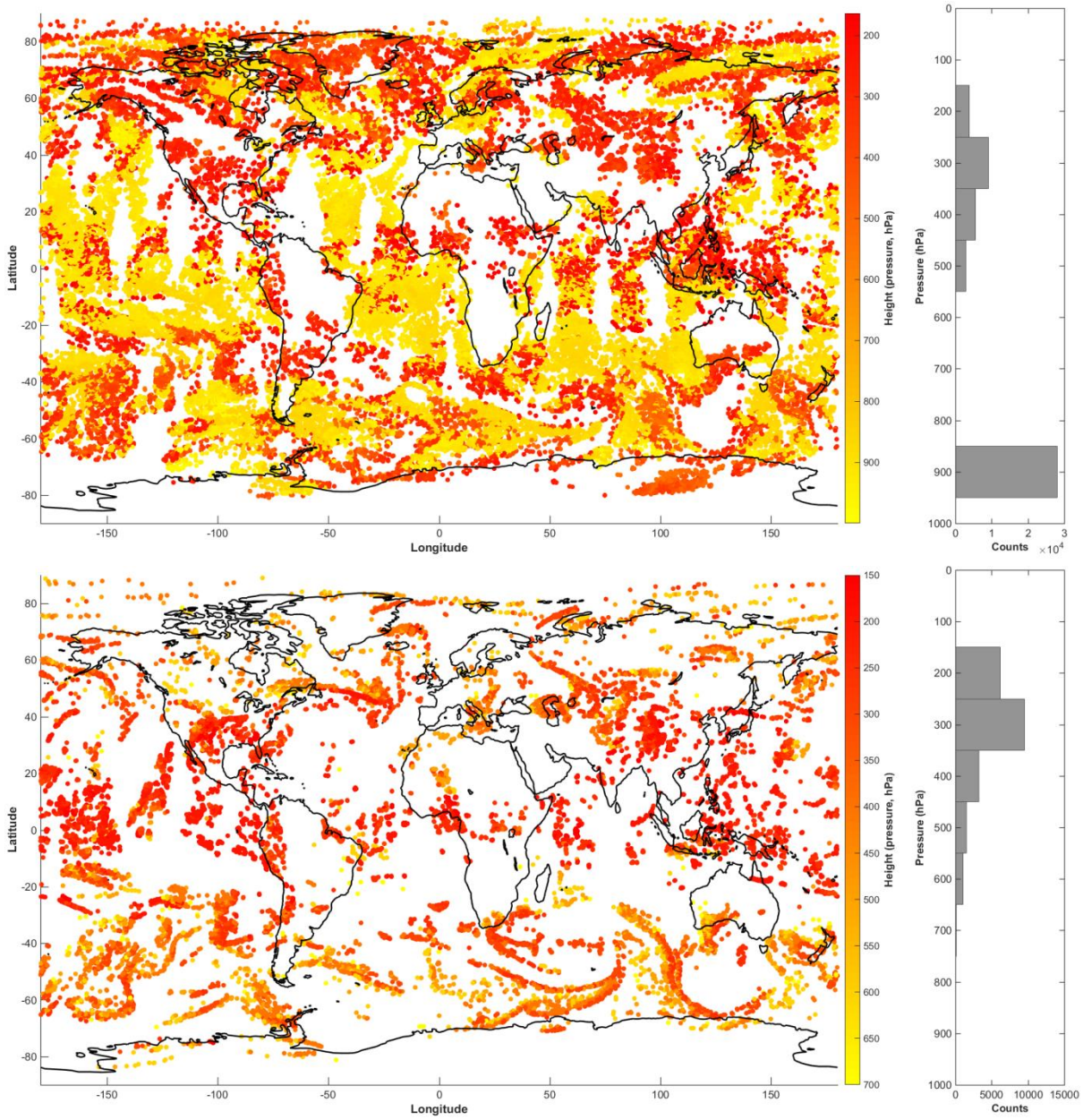

Figure 10 – MISTiC™ Winds simulated cloud (top) and water vapor (bottom) AMVs' spatial (left) and vertical (right) distributions for one 6-hour window with 4 orbital planes.

The estimated MISTiC™ AMV locations for the four orbit planes configuration are shown in Figure 10 for the six-hour assimilation cycle centered on 0000 UTC for G5NR date 1 July 2006. Using this algorithm, MISTiC™ Winds is estimated to be able to collect 51,598 cloud and 21,737 water vapor AMVs.

The estimated cloud AMV locations (Fig 10, top panel) show a vertical distribution close to what is to be expected, similar to the ones currently seen for the AMVs derived from operating satellites:

a bimodal vertical distribution with maxima corresponding to high clouds (ranging from 200 to 400 hPa) and low clouds (from 800 to 1000 hPa). For the estimated water vapor AMVs, the vertical distribution (Figure 10, bottom panel) reflects the expected added-value of MISTiC™ Winds in terms of increased vertical resolution; specifically, the simulated AMV distributions extend below 400 hPa. However, the maximum observational count will still occur at higher atmospheric levels (200-300 hPa) as it does with the current water vapor feature tracking AMVs, due to the nature of cloud contamination in the retrieval process. While the additional mid-level information is partially by construction, due to the pre-specification of the isobaric retrieval layers, estimating the positions of these observations is fundamental to their assessment in an OSSE. The water vapor AMV counts' gradual downward tapering through the troposphere were tuned towards the results of the methods proposed in Santek et al. (2014). This distribution could likely be further refined for a more globally-representative distribution.

Qualitatively, Figure 10 (bottom) shows gaps in water vapor AMV locations that spatially correspond to the presence of dense cloud features located above the water vapor features, as inferred from the cloud AMV (Fig. 10, top). The upper cloud features obscure the water vapor features located below them. The MISTiC™ instruments will be unable to detect water vapor features through opaque clouds. Also in Figure 10 (bottom panel), one is able to see frontal features corresponding to the presence of water vapor AMVs.

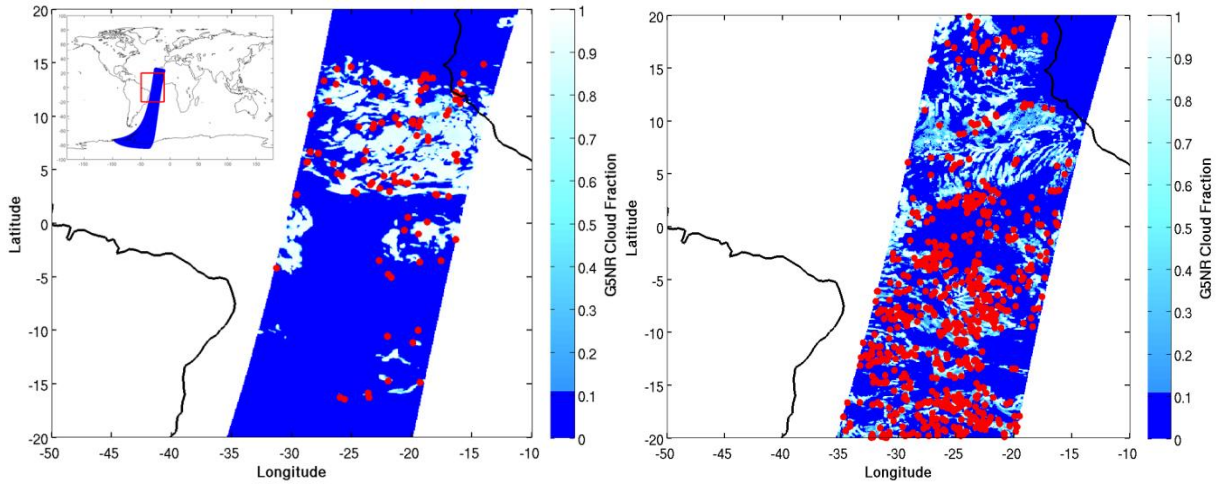

Figure 11 – Estimated MISTiC Winds cloud AMV locations overlapped with G5NR cloud fraction field at 200 hPa (left) and 900 hPa (right) for 1 July 00:30 UTC, zoomed for an orbit segment (upper left subplot).

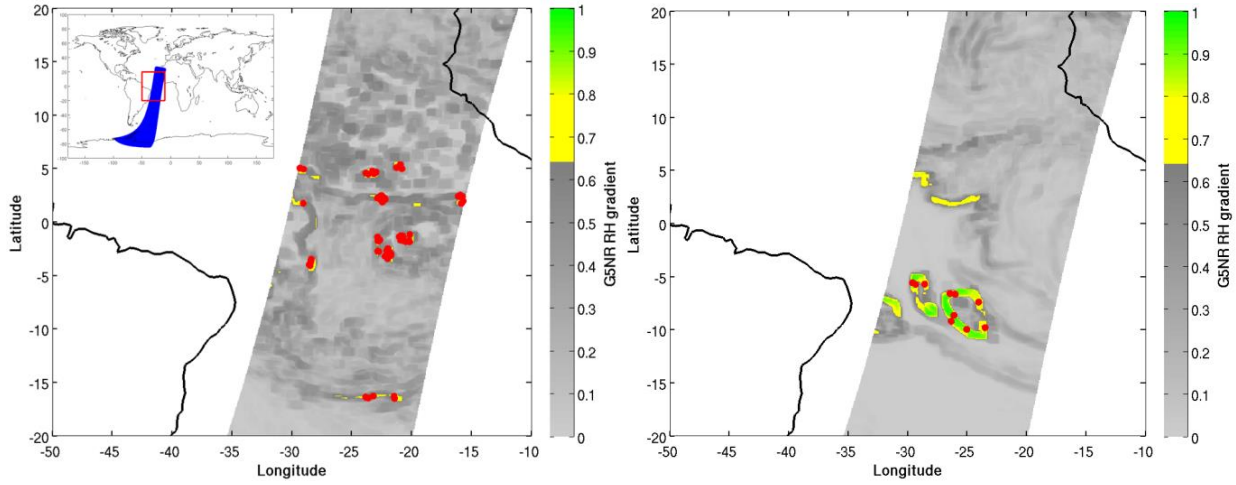

Figure 12 – Estimated MISTiC Winds water vapor AMV locations and G5NR relative humidity gradient field at 200 hPa (left) and 600 hPa (right) for 1 July 00:30 UTC, zoomed for an orbit segment (upper left subplot).

Figures 11 and 12 show examples of the estimated MISTiC Winds cloud and water vapor AMV locations (red dots) overlapped with the G5NR CF and RH_{grad} fields for 1 July 2006 0030 UTC. In both figures, a segment of the MISTiC Winds orbit was chosen, as depicted in the upper left sub-plot of each figure. Estimated AMV locations contained in two 50 hPa vertical layers centered at 200 and 900 hPa (for the cloud AMVs in Figure 11) and at 200 and 600 hPa (for the water vapor AMVs in Figure 12) are shown.

Figure 11 shows that the estimated cloud AMV locations are mainly found at G5NR points with fractional cloud cover, for which cloud edges should be more discernible. There is a much higher number of cloud AMV locations at the 900 hPa layer than at the 200 hPa layer, not only because there appears to be more clouds at 900 hPa than at 200 hPa, but also because the CAMV probability function b(p) was tuned to allow more observations at 900 hPa. Figure 8 showed that AHI cloud AMVs have their count maxima at this level. Oppositely, b(p) was adjusted in accordance to AHI cloud AMV counts at 200 hPa, resulting in a lower observation density at this level, even in the presence of clouds.

For the water vapor AMVs (Figure 12), practically all the trackable water vapor features (RH_{grad} higher than 65%) at 200 hPa are selected by the P_{wv}, whereas at 600 hPa only some of them are. At 200 hPa, the probability of the water vapor features being covered by clouds from above is very low, and thus P_{wv} provides a very high probability of being an effective AMV location. Moreover, the 200 hPa cloud and water vapor AMV locations are qualitatively correlated spatially, since the cloud fraction and RH_{grad} fields are closely related; cloud edges are, after all, fundamentally water vapor gradients. Figure 12 also shows that the 600 hPa water vapor AMVs, although at a low-level, are present in areas of clear sky; this constitutes additional information provided by the MISTiC™ Winds observing strategy.

Figure 11 shows many areas with intermediate cloud fractions that do not contain any AMVs, whereas other areas, with smaller or larger cloud fractions, do contain some observations. Figure 12 shows areas with high RH_{grad} which do not contain any observations. As previously discussed for Figures 6 and 7, this is due to the nature and design of the probabilistic functions, the possibility of features being obscured by clouds aloft, and, in the case of the cloud-tracking AMVs, the AMV height assignment method.

6 - Conclusions

A tunable and flexible algorithm to estimate the locations and spatial distributions of AMVs, as would be derived from different instruments and satellite orbit configurations specifically for OSSE applications, has been developed for use in the GMAO OSSE framework. The algorithm first identifies AMV tracers in a NR. The algorithm then employs a probabilistic function to select a subset of these identified trackable features as estimates of AMV locations, which can later be easily used to derive synthetic AMV observations for use in OSSEs. The main motivation for this work was the need to produce simulated AMVs that are located in areas of the NR where AMV tracers are expected to exist. With the described algorithm, there is now the capability to use AMVs simulated with physical realism within OSSEs, allowing the estimation and quantification of the potential added value of new observing strategies in the context of the present global observing system, at the same time quantifying their effectiveness, strengths, and potential shortcomings.

The Himawari-8 AHI cloud and water vapor AMVs were used in this work to perform a qualitative assessment of the AMV algorithm. The assessment was used to determine if the estimated AMV locations were coincident with trackable feature locations in the NR and also if they yielded realistic AMV observations counts and spatial distributions. The estimated AHI cloud and water vapor AMV locations did show a good match with the actual AHI AMV locations in terms of observation counts and spatial distributions. The horizontal distributions showed some differences in terms of the locations of the observation counts' maxima and minima due to differences between the real and G5NR-simulated cloud and water vapor fields.

To illustrate the effectiveness of this tool, it was applied to the MISTiC™ Winds concept. This component of the work was performed as part of a set of OSSEs to investigate the utility of the constellation (McCarty et al., 2018). When applied to MISTiC™, the algorithm produces an estimated water vapor AMV vertical distribution that reflects the expected added-value of the MISTiC™ strategy in terms of increased vertical resolution, being able to derive AMVs below 400 hPa. This is a fundamentally unique feature of the MISTiC™ Winds strategy compared to those strategies currently in use with the modern global observing system. Ultimately, the algorithm presented here provides an idea as to how the MISTiC™ Winds AMV measurements will be distributed as a function of the constellation configuration.

Acknowledgements

This effort was funded by NASA Headquarters through both the Modeling, Analysis, and Prediction program and the Earth Science Technology Office. Computational resources were provided by the NASA Center for Climate Simulation. The authors would like to acknowledge the valuable contributions of Ron Errico and Nikki Prive (NASA GMAO) to this work, mainly related to the use and adaptation of methodologies and algorithms of NASA's GMAO OSSE code.

References

Borde, R., M. Doutriaux-Boucher, G. Dew, and M. Carranza, 2014: A direct link between feature tracking and height assignment of operational EUMETSAT atmospheric motion vectors. J. Atmos. Oceanic Technol., 31, 33–46

Boukabara SA, and Coauthors (2016). Community global observing system simulation experiment (OSSE) package (CGOP): Description and usage. J. Atmos. Oceanic Technol., 33, 1759–1777

Boukabara SA, and Coauthors (2018a). Community global observing system simulation experiment (OSSE) package (CGOP): Perfect observations simulation validation. J. Atmos. Oceanic Technol., 35, 207–226

Boukabara SA, and Coauthors (2018b). Community global observing system simulation experiment (OSSE) package (CGOP): Assessment and validation of the OSSE system using an OSSE–OSE intercomparison of summary assessment metrics. J. Atmos. Oceanic Technol., 35, 2061–2078

Cordoba, M., Dance, S. L., Kelly, G. A., Nichols, N. K., Waller, J. A. (2016). Diagnosing atmospheric motion vector observation errors for an operational high-resolution data assimilation system. Quarterly Journal of the Royal Meteorological Society, 143(702), Part A, 333-341.

Errico RM, Ohring G, Bauer P, Ferrier B, Mahfouf J-F, Turk J, Weng F (2007): Assimilation of satellite cloud and precipitation observations in numerical weather prediction models: Introduction to the JAS Special Collection. Journal of Atmospheric Science, 64, 3737-3741

Errico RM, Yang R, Privé NC, Tai KS, Todling R, Sienkiewicz ME, Guo J. (2013): Development and validation of observing-system simulation experiments at NASA's Global Modeling and Assimilation Office. Quarterly Journal of the Royal Meteorological Society, 139(674), Part A, 1162-1178

Errico RM, Privé NC (2014): An estimate of some analysis error statistics using the GMAO observing system simulation framework. Quarterly Journal of the Royal Meteorological Society, 140, 1005-1012

Errico RM, Privé NC, Carvalho D, Sienkiewicz M, Todling M, McCarty W , Guo J, El Akkraoui A, Putman WM, da Silva A, Gelaro R, Moradi I (2016): Description of the GMAO OSSE for Weather Analysis Software Package: Version 3. NASA Technical Report.

Forsythe M (2007): Atmospheric motion vectors: past, present and future. ECMWF Annual Seminar, Met Office, Exeter, UK

Gelaro R, Putman WM, Pawson S, Draper C, Molod A, Norris PM, Ott L, Privé N, Reale O, Achuthavarier D, Bosilovich M, Buchard V, Chao W, Coy L, Cullather R, da Silva A, Darmenov A, Errico RM, Fuentes M, Kim M-J, Koster R, McCarty W, Nattala J, Partyka G, Schubert S, Vernieres G, Vikhliaev Y, Wargan K (2015): Evaluation of the 7-km GEOS-5 Nature Run. NASA Technical Report, NASA/TM-2014-104606/VOL36, GSFC-E-DAA-TN21523

Gelaro R, et al. (2016): The Modern-Era Retrospective Analysis for Research and Applications, Version 2 (MERRA-2). Journal of Climate, Special MERRA-2 Collection, 30, 5419-5454

Goerss J, Velden C, Hawkins J (1998): The Impact of Multispectral GOES-8 Wind Information on Atlantic Tropical Cyclone Track Forecasts in 1995. Part 2: NOGAPS Forecasts. Monthly Weather Reviews, 126, 1219-1227

Hoffman, RN, Atlas R (2016). Future observing system simulation experiments. Bulletin of the American Meteorological Society, 97, 1601–1616

Kleist D, Parrish D, Derber J, Treadon R, Wu W-S, Lord S (2009): Introduction of the GSI into the NCEP global data assimilation system. Weather and Forecasting, 24, 1691-1705

Lazzara MA, Dworak R, Santek D, Hoover BT, Velden CS, Key JR (2013): High-Latitude Atmospheric Motion Vectors from Composite Satellite Data. Journal of Applied Meteorology and Climatology, 53, 534-547

Lean, K., Salonen, K., Bormann, B. (2016). Assessment of AMVs from Himawari-8 and VIIRS. Proceedings for the 13th International Winds Workshop 27 June - 1 July 2016, Monterey, California, USA.

Maschhoff KR, Polizotti JJ, Aumann HH, Susskind J (2016): MISTiC™ winds, a microsatellite constellation approach to high-resolution observations of the atmosphere using infrared sounding and 3D winds measurements. Proceedings of the SPIE Vol. 9978, 997804-1

Masutani M, Riishojgaard LP, Woollen JS, Casey S (2012). Observing system simulation experiments at Joint Center for Satellite Data Assimilation. Proceedings of SPIE - The International Society for Optical Engineering, Vol. 8529, Article number 85290B. Remote Sensing and Modeling of the Atmosphere, Oceans, and Interactions IV, Kyoto, Japan, 31 October - 1 November 2012; Code 104953

McCarty W, Errico RM, Yang R, Gelaro R, Rienecker M (2011). The simulation and assimilation of Doppler wind lidar observations in support of future instruments. 91st AMS Annual Meeting, January 22–27 2011, Seattle, USA.

McCarty W, Errico RM, Gelaro R (2012): Cloud Coverage in the Joint OSSE Nature Run. Monthly Weather Review, 140, 1863-1871

McCarty W, Blaisdell J, Carvalho D, Errico R, Gelaro R, Kouvaris L, Moradi I, Pawson S, Prive N, Sienkiewicz ME, Susskind J (2017). Progress Towards an OSSE Investigating a Constellation of 4-5 μm Infrared Sounders. 97th AMS Annual Meeting, January 22–26 2017, Seattle, USA.

McCarty W, J. Blaisdell, M. Cordero-Fuentes, D. Carvalho, R. Errico, R. Gelaro, L. Kouvaris, I. Moradi, S. Pawson, N. Prive (2018). A GEOS-Based OSSE for the MISTiC Winds Concept. Working Group on Space-Based Lidar Winds, 7-8 Feb. 2018, Boulder, CO, United States. http://hdl.handle.net/2060/20180001303

McNally AP (2002): A note on the occurrence of cloud in meteorologically sensitive areas and the implications for advanced infrared sounders. Quarterly Journal of the Royal Meteorological Society, 128, 2551-2556

Molod A, Kim M-J, Nattala J, Bosilovich M, Schubert S, Chao W (2015): Humidity and precipitation. Evaluation of the 7-km GEOS-5 nature run, R. D. Koster, Ed., NASA/TM-2014-104606, Tech. Rep. Series on Global Modeling and Data Assimilation, Vol. 36, 67–112.

Norris P, McCarty W, Errico R (2015): Clouds and radiation. Evaluation of the 7-km GEOS-5 nature run, R. D. Koster, Ed., NASA/TM-2014-104606, Tech. Rep. Series on Global Modeling and Data Assimilation, Vol. 36, 192–112.

Privé NC, Errico RM, Tai KS. (2013): Validation of the forecast skill of the Global Modeling and Assimilation Office observing system simulation experiment. Quarterly Journal of the Royal Meteorological Society, 139, 1354–1363

Privé NC, Coy L, Errico RM (2015): Wind and temperature. Evaluation of the 7-km GEOS-5 nature run, R. D. Koster, Ed., NASA/TM-2014-104606, Tech. Rep. Series on Global Modeling and Data Assimilation, Vol. 36, 30–66.

Putman WM (2015): Overview. Evaluation of the 7-km GEOS-5 nature run, R. D. Koster, Ed., NASA/TM-2014-104606, Tech. Rep. Series on Global Modeling and Data Assimilation, Vol. 36, 1–29.

Rienecker M, Suarez M, Todling R, Bacmeister J, Takacs L, Liu H-C, Gu W, Sienkiewicz M, Koster R, Gelaro R, Stajner I, Nielsen J (2008): The GEOS-5 data assimilation system - documentation of versions 5.0.1, 5.1.0 and 5.2.0, Technical Report 27, NASA

Santek D, Nebuda S, Stettner D (2014). Feature-tracked Winds from Moisture Fields Derived from AIRS Sounding Retrievals. IWW12 Twelfth International Winds Workshop, 16-20 June 2014, Copenhagen, Denmark.

Soden BJ, Velden C, Tuleya R (2001): The Impact of Satellite Winds on Experimental GFDL Hurricane Model Forecasts. Monthly Weather Reviews, 129, 835-852

Szantai, A., F. Désalmand, M. Desbois, P. Lecomte, E. Mémin and S. Zimeras, 2000: Tracking low-level clouds over Central Africa on Meteosat images. In 2000 EUMETSAT Meteorological Satellite Data Users' Conference. Bologna, Italy (29 May - 2 June 2000). EUMETSAT, EUM P 29, 813-820.

Tian L, Curry JA (1989). Cloud overlap statistics, Journal of Geophysical Research, 94, 9925–9935.

Velden C, Bedka K (2009). Identifying the Uncertainty in Determining Satellite-Derived Atmospheric Motion Vector Height Attribution. Journal of Applied Meteorology and Climatology, 48, 450-463.

Wylie DP, Menzel WP (1999). Eight years of high cloud statistics using HIRS. Journal of Climate, 12, 170–184

Previous Volumes in This Series

Volume 1 September 1994	Documentation of the Goddard Earth Observing System (GEOS) general circulation model - Version 1 **L.L. Takacs, A. Molod, and T. Wang**
Volume 2 October 1994	Direct solution of the implicit formulation of fourth order horizontal diffusion for gridpoint models on the sphere **Y. Li, S. Moorthi, and J.R. Bates**
Volume 3 December 1994	An efficient thermal infrared radiation parameterization for use in general circulation models **M.-D. Chou and M.J. Suarez**
Volume 4 January 1995	Documentation of the Goddard Earth Observing System (GEOS) Data Assimilation System - Version 1 **James Pfaendtner, Stephen Bloom, David Lamich, Michael Seablom, Meta Sienkiewicz, James Stobie, and Arlindo da Silva**
Volume 5 April 1995	Documentation of the Aries-GEOS dynamical core: Version 2 **Max J. Suarez and Lawrence L. Takacs**
Volume 6 April 1995	A Multiyear Assimilation with the GEOS-1 System: Overview and Results **Siegfried Schubert, Chung-Kyu Park, Chung-Yu Wu, Wayne Higgins, Yelena Kondratyeva, Andrea Molod, Lawrence Takacs, Michael Seablom, and Richard Rood**
Volume 7 September 1995	Proceedings of the Workshop on the GEOS-1 Five-Year Assimilation **Siegfried D. Schubert and Richard B. Rood**
Volume 8 March 1996	Documentation of the Tangent Linear Model and Its Adjoint of the Adiabatic Version of the NASA GEOS-1 C-Grid GCM: Version 5.2 **Weiyu Yang and I. Michael Navon**
Volume 9 March 1996	Energy and Water Balance Calculations in the Mosaic LSM **Randal D. Koster and Max J. Suarez**

Volume 10 April 1996	Dynamical Aspects of Climate Simulations Using the GEOS General Circulation Model **Lawrence L. Takacs and Max J. Suarez**
Volume 11 May 1997	Documentation of the Tangent Linear and Adjoint Models of the Relaxed Arakawa-Schubert Moisture Parameterization Package of the NASA GEOS-1 GCM (Version 5.2) **Weiyu Yang, I. Michael Navon, and Ricardo Todling**
Volume 12 August 1997	Comparison of Satellite Global Rainfall Algorithms **Alfred T.C. Chang and Long S. Chiu**
Volume 13 December 1997	Interannual Variability and Potential Predictability in Reanalysis Products **Wie Ming and Siegfried D. Schubert**
Volume 14 August 1998	A Comparison of GEOS Assimilated Data with FIFE Observations **Michael G. Bosilovich and Siegfried D. Schubert**
Volume 15 June 1999	A Solar Radiation Parameterization for Atmospheric Studies **Ming-Dah Chou and Max J. Suarez**
Volume 16 November 1999	Filtering Techniques on a Stretched Grid General Circulation Model **Lawrence Takacs, William Sawyer, Max J. Suarez, and Michael S. Fox-Rabinowitz**
Volume 17 July 2000	Atlas of Seasonal Means Simulated by the NSIPP-1 Atmospheric GCM **Julio T. Bacmeister, Philip J. Pegion, Siegfried D. Schubert, and Max J. Suarez**
Volume 18 December 2000	An Assessment of the Predictability of Northern Winter Seasonal Means with the NSIPP1 AGCM **Philip J. Pegion, Siegfried D. Schubert, and Max J. Suarez**
Volume 19 July 2001	A Thermal Infrared Radiation Parameterization for Atmospheric Studies **Ming-Dah Chou, Max J. Suarez, Xin-Zhong Liang, and Michael M.-H. Yan**
Volume 20 August 2001	The Climate of the FVCCM-3 Model

	Yehui Chang, Siegfried D. Schubert, Shian-Jiann Lin, Sharon Nebuda, and Bo-Wen Shen
Volume 21 September 2001	Design and Implementation of a Parallel Multivariate Ensemble Kalman Filter for the Poseidon Ocean General Circulation Model **Christian L. Keppenne and Michele M. Rienecker**
Volume 22 August 2002	A Coupled Ocean-Atmosphere Radiative Model for Global Ocean Biogeochemical Models **Watson W. Gregg**
Volume 23 November 2002	Prospects for Improved Forecasts of Weather and Short-term Climate Variability on Subseasonal (2-Week to 2-Month) Time Scales **Siegfried D. Schubert, Randall Dole, Huang van den Dool, Max J. Suarez, and Duane Waliser**
Volume 24 July 2003	Temperature Data Assimilation with Salinity Corrections: Validation for the NSIPP Ocean Data Assimilation System in the Tropical Pacific Ocean, 1993–1998 **Alberto Troccoli, Michele M. Rienecker, Christian L. Keppenne, and Gregory C. Johnson**
Volume 25 December 2003	Modeling, Simulation, and Forecasting of Subseasonal Variability **Duane Waliser, Siegfried D. Schubert, Arun Kumar, Klaus Weickmann, and Randall Dole**
Volume 26 April 2005	Documentation and Validation of the Goddard Earth Observing System (GEOS) Data Assimilation System – Version 4 **Senior Authors: S. Bloom, A. da Silva and D. Dee** **Contributing Authors: M. Bosilovich, J-D. Chern, S. Pawson, S. Schubert, M. Sienkiewicz, I. Stajner, W-W. Tan, and M-L. Wu**
Volume 27 December 2008	The GEOS-5 Data Assimilation System - Documentation of Versions 5.0.1, 5.1.0, and 5.2.0. **M.M. Rienecker, M.J. Suarez, R. Todling, J. Bacmeister, L. Takacs, H.-C. Liu, W. Gu, M. Sienkiewicz, R.D. Koster, R. Gelaro, I. Stajner, and J.E. Nielsen**
Volume 28 April 2012	The GEOS-5 Atmospheric General Circulation Model: Mean Climate and Development from MERRA to Fortuna

	Andrea Molod, Lawrence Takacs, Max Suarez, Julio Bacmeister, In-Sun Song, and Andrew Eichmann
Volume 29	Atmospheric Reanalyses – Recent Progress and Prospects for the Future.
June 2012	A Report from a Technical Workshop, April 2010
	Michele M. Rienecker, Dick Dee, Jack Woollen, Gilbert P. Compo, Kazutoshi Onogi, Ron Gelaro, Michael G. Bosilovich, Arlindo da Silva, Steven Pawson, Siegfried Schubert, Max Suarez, Dale Barker, Hirotaka Kamahori, Robert Kistler, and Suranjana Saha
Volume 30	The GEOS-iODAS: Description and Evaluation
December 2012	**Guillaume Vernieres, Michele M. Rienecker, Robin Kovach and Christian L. Keppenne**
Volume 31	Global Surface Ocean Carbon Estimates in a Model Forced by MERRA
March 2013	**Watson W. Gregg, Nancy W. Casey and Cecile S. Rousseaux**
Volume 32	Estimates of AOD Trends (2002-2012) over the World's Major Cities based on the MERRA Aerosol Reanalysis
March 2014	**Simon Provencal, Pavel Kishcha, Emily Elhacham, Arlindo M. da Silva, and Pinhas Alpert**
Volume 33	The Effects of Chlorophyll Assimilation on Carbon Fluxes in a Global Biogeochemical Model
August 2014	**Cécile S. Rousseaux and Watson W. Gregg**
Volume 34	Background Error Covariance Estimation using Information from a Single Model Trajectory with Application to Ocean Data Assimilation into the GEOS-5 Coupled Model
September 2014	**Christian L. Keppenne, Michele M. Rienecker, Robin M. Kovach, and Guillaume Vernieres**
Volume 35	Observation-Corrected Precipitation Estimates in GEOS-5
December 2014	**Rolf H. Reichle and Qing Liu**
Volume 36	Evaluation of the 7-km GEOS-5 Nature Run
March 2015	**Ronald Gelaro, William M. Putman, Steven Pawson, Clara Draper, Andrea Molod, Peter M. Norris, Lesley Ott, Nikki Prive, Oreste Reale, Deepthi Achuthavarier, Michael Bosilovich, Virginie Buchard, Winston Chao, Lawrence Coy, Richard Cullather, Arlindo da Silva, Anton Darmenov, Ronald M. Errico, Marangelly Fuentes, Min-Jeong**

	Kim, Randal Koster, Will McCarty, Jyothi Nattala, Gary Partyka, Siegfried Schubert, Guillaume Vernieres, Yuri Vikhliaev, and Krzysztof Wargan
Volume 37 March 2015	Maintaining Atmospheric Mass and Water Balance within Reanalysis **Lawrence L. Takacs, Max Suarez, and Ricardo Todling**
Volume 38 September 2015	The Quick Fire Emissions Dataset (QFED) – Documentation of versions 2.1, 2.2 and 2.4 **Anton S. Darmenov and Arlindo da Silva**
Volume 39 September 2015	Land Boundary Conditions for the Goddard Earth Observing System Model Version 5 (GEOS-5) Climate Modeling System - Recent Updates and Data File Descriptions **Sarith Mahanama, Randal Koster, Gregory Walker, Lawrence Takacs**, **Rolf** **Reichle, Gabrielle De Lannoy, Qing Liu, Bin Zhao, and** Max **Suarez**
Volume 40 October 2015	Soil Moisture Active Passive (SMAP) Project Assessment Report for the Beta-Release L4_SM Data Product **Rolf H. Reichle, Gabrielle J. M. De Lannoy, Qing Liu, Andreas Colliander**, **Austin Conaty, Thomas Jackson, John Kimball, and Randal D. Koster**
Volume 41 October 2015	GDIS Workshop Report **Siegfried Schubert, Will Pozzi, Kingtse Mo, Eric Wood, Kerstin Stahl, Mike Hayes, Juergen Vogt, Sonia Seneviratne, Ron Stewart, Roger Pulwarty, and Robert Stefanski**
Volume 42 November 2015	Soil Moisture Active Passive (SMAP) Project Calibration and Validation for the L4_C Beta-Release Data Product **John Kimball, Lucas Jones, Joseph Glassy, E. Natasha Stavros, Nima Madani, Rolf Reichle, Thomas Jackson, and Andreas Colliander**
Volume 43 September 2015	MERRA-2: Initial Evaluation of the Climate **Michael G. Bosilovich, Santha Akella, Lawrence Coy, Richard Cullather, Clara Draper, Ronald Gelaro, Robin Kovach, Qing Liu, Andrea Molod, Peter Norris, Krzysztof Wargan, Winston Chao, Rolf Reichle, Lawrence Takacs, Yury Vikhliaev, Steve Bloom, Allison Collow, Stacey Firth, Gordon Labow, Gary Partyka, Steven Pawson, Oreste Reale, Siegfried Schuber**t, **and Max Suarez**

Volume 44 February 2016	Estimation of the Ocean Skin Temperature using the NASA GEOS Atmospheric Data Assimilation System **Santha Akella, Ricardo Todling, Max Suarez**
Volume 45 October 2016	The MERRA-2 Aerosol Assimilation **C. A. Randles, A. M. da Silva, V. Buchard, A. Darmenov, P. R. Colarco, V. Aquila, H. Bian, E. P. Nowottnick, X. Pan, A. Smirnov, H. Yu, and R. Govindaraju**
Volume 46 October 2016	The MERRA-2 Input Observations: Summary and Assessment **Will McCarty, Lawrence Coy, Ronald Gelaro, Albert Huang, Dagmar Merkova, Edmond B. Smith, Meta Sienkiewicz, and Krzysztof Wargan**
Volume 47 **May 2017**	An Evaluation of Teleconnections Over the United States in an Ensemble of AMIP Simulations with the MERRA-2 Configuration of the GEOS Atmospheric Model. Allison B. Marquardt Collow, Sarith P. Mahanama, Michael G. Bosilovich, Randal D. Koster, and Siegfried D. Schubert
Volume 48 **July 2017**	Description of the GMAO OSSE for Weather Analysis Software Package: Version 3 Ronald M. Errico, Nikki C. Prive, David Carvalho, Meta Sienkiewicz, Amal El Akkraoui, Jing Guo, Ricardo Todling, Will McCarty, William M. Putman, Arlindo da Silva, Ronald Gelaro, and Isaac Moradi
Volume 49 **March 2018**	Preliminary Evaluation of Influence of Aerosols on the Simulation of Brightness Temperature in the NASA Goddard Earth Observing System Atmospheric Data Assimilation System Jong Kim, Santha Akella, Will McCarty, Ricardo Todling, and Arlindo M. da Silva
Volume 50 **March 2018**	The GMAO Hybrid Ensemble-Variational Atmospheric Data Assimilation System: Version 2.0 Ricardo Todling and Amal El Akkraoui
Volume 51 **July 2018**	The Atmosphere-Ocean Interface Layer of the NASA Goddard Earth Observing System Model and Data Assimilation System Santha Akella and Max Suarez

Volume 52 **July 2018**	Soil Moisture Active Passive (SMAP) Project Assessment Report for Version 4 of the L4_SM Data Product Rolf H. Reichle, Qing Liu, Randal D. Koster, Joe Ardizzone, Andreas Colliander, Wade Crow, Gabrielle J. M. De Lannoy, and John Kimball
Volume 53 **October 2019**	Ensemble Generation Strategies Employed in the GMAO GEOS-S2S Forecast System Siegfried Schubert, Anna Borovikov, Young-Kwon Lim, and Andrea Molod